

Measurement of τ polarization
in e^+e^- annihilation at $\sqrt{s}=58$ GeV

H. Hanai *et al.*

VENUS Collaboration

The polarization of τ leptons in the reaction $e^+e^- \rightarrow \tau^+\tau^-$ has been measured using a e^+e^- collider, TRISTAN, at the center-of-mass energy of 58 GeV. From the kinematical distributions of daughter particles in $\tau \rightarrow e\nu\bar{\nu}$, $\mu\nu\bar{\nu}$, $\rho\nu$ or $\pi(K)\nu$ decays, the average polarization of τ^- and its forward-backward asymmetry have been evaluated to be 0.012 ± 0.058 and 0.029 ± 0.057 , respectively.

(Submitted to Phys. Lett. B)

H. Hanai^{1,a}, J. Haba², K. Abe³, K. Amako², Y. Arai², T. Arima^{4,b}, Y. Asano⁴, M. Chiba⁵, Y. Chiba⁶, M. Daigo⁷, M. Fukawa^{2,c}, Y. Fukushima², H. Hamasaki⁴, Y. Hemmi⁸, M. Higuchi⁹, T. Hirose⁵, Y. Homma¹⁰, N. Hosoda^{5,d}, N. Ishihara², Y. Iwata¹¹, J. Kanzaki², R. Kikuchi⁸, T. Kondo², T. T. Korhonen^{2,12,e}, H. Kurashige⁸, E. K. Matsuda¹³, T. Matsui², M. Miura^{4,f}, K. Miyake⁸, S. Mori⁴, Y. Nagashima¹, Y. Nakagawa^{14,g}, T. Nakamura^{15,h}, I. Nakano^{16,i}, S. Odaka², K. Ogawa^{2,h}, T. Ohama², T. Ohsugi¹¹, H. Ohyama¹⁷, K. Okabe¹³, A. Okamoto⁸, A. Ono¹⁸, J. Pennanen^{2,12}, H. Sakamoto⁸, M. Sakuda², M. Sato⁹, N. Sato², M. Shioden¹⁹, J. Shirai², T. Sumiyoshi², Y. Takada⁴, -F. Takasaki², M. Takita¹, N. Tamura^{13,j}, D. Tatsumi¹, K. Tobimatsu²⁰, T. Tsuboyama², S. Uehara², Y. Unno², T. Watanabe²¹, Y. Watase², F. Yabuki⁵, Y. Yamada², T. Yamagata¹⁴, Y. Yonezawa²², H. Yoshida²³ and K. Yusa⁴

¹Department of Physics, Osaka University, Toyonaka 560, Japan

²KEK, National Laboratory for High Energy Physics, Tsukuba 305, Japan

³Department of Physics, Tohoku University, Sendai 980, Japan

⁴Institute of Applied Physics, University of Tsukuba, Tsukuba 305, Japan

⁵Department of Physics, Tokyo Metropolitan University, Hachioji 192-03, Japan

⁶Yasuda Women's Junior College, Hiroshima 731-01, Japan

⁷Faculty of Economics, Toyama University, Toyama 930, Japan

⁸Department of Physics, Kyoto University, Kyoto 606, Japan

⁹Department of Applied Physics, Tohoku-Gakuin University, Tagajo 985, Japan

¹⁰Faculty of Engineering, Kobe University, Kobe 657, Japan

¹¹Department of Physics, Hiroshima University, Higashi-Hiroshima 724, Japan

¹²Research Institute for High Energy Physics, Helsinki University, SF-00170 Helsinki, Finland

¹³Department of Physics, Okayama University, Okayama 700, Japan

¹⁴International Christian University, Mitaka 181, Japan

¹⁵Faculty of Engineering, Miyazaki University, Miyazaki 889-01, Japan

¹⁶Institute of Physics, University of Tsukuba, Tsukuba 305, Japan

¹⁷Hiroshima National College of Maritime Technology, Higashino 725-02, Japan

¹⁸Faculty of Cross-Cultural Studies, Kobe University, Kobe 657, Japan

¹⁹Ibaraki College of Technology, Katsuta 312, Japan

²⁰Center for Information Science, Kogakuin University, Tokyo 163-91, Japan

²¹Department of Physics, Kogakuin University, Hachioji 192, Japan

²²Tsukuba College of Technology, Tsukuba 305, Japan

²³Naruto University of Education, Naruto 772, Japan

^aPresent address: ASTEC Inc., BR Ichigaya, 6 Minami-cho, Shinjuku-ku, Tokyo 162, Japan.

^bPresent address: Faculty of Engineering, Kyushu University, Fukuoka 812, Japan.

^cPresent address: Naruto University of Education, Naruto 772, Japan.

^dPresent address: Japan Synchrotron Radiation Research Institute, Kamigouri 678-12, Japan.

^ePresent address: Accelerator Division, KEK, Tsukuba 305, Japan.

^fPresent address: Institute for Cosmic Ray Research, University of Tokyo, Tanashi 188, Japan.

^gPresent address: Department of Mathematical Sciences, Ehime University, Matsuyama 790-77, Japan.

^hDeceased.

ⁱPresent address: Department of Physics, Okayama University, Okayama 700, Japan.

^jPresent address: Department of Physics, Niigata University, Niigata 950-21, Japan.

1 Introduction

The polarization of τ leptons in the reaction,

$$e^+e^- \rightarrow \tau^+\tau^- \quad (1)$$

provides us with information concerning the properties of the neutral current of leptons [1]. The measurement of it is, therefore, important in every Q^2 range of the reaction.

The average polarization of τ leptons is defined as

$$\mathcal{P}_\tau = \frac{\sigma(h = +1) - \sigma(h = -1)}{\sigma(h = +1) + \sigma(h = -1)}, \quad (2)$$

where $h(= \pm 1)$ is the helicity of τ^- . Another relevant observable is the forward-backward asymmetry of the polarization defined as

$$A_{\mathcal{P}} = \frac{\sigma_F \mathcal{P}_F - \sigma_B \mathcal{P}_B}{\sigma_F + \sigma_B}, \quad (3)$$

where \mathcal{P}_F and \mathcal{P}_B are the average polarizations measured in the forward and backward regions, respectively, relative to the incoming e^- direction.

Although there are many precise measurements on \mathcal{P}_τ and $A_{\mathcal{P}}$ at Z^0 pole [2], very few are available below the pole [3]. Besides, the previous measurements below the pole suffered from relatively large statistical errors due to the small cross section of reaction (1).

This letter describes a measurement of \mathcal{P}_τ and $A_{\mathcal{P}}$ at a center-of-mass energy (\sqrt{s}) of 58 GeV using the VENUS detector at TRISTAN. The analysis is based on the data corresponding to an integrated luminosity of 271 pb $^{-1}$.

In the framework of the Standard Model [4], the differential cross section of the reaction (1) can be expressed for unpolarized electron and positron as

$$\frac{d\sigma}{d\Omega}(\cos\theta, h) = \frac{\alpha^2}{8s} [F_0(s)(1 + \cos^2\theta) + 2F_1(s)\cos\theta - h\{F_2(s)(1 + \cos^2\theta) + 2F_3(s)\cos\theta\}], \quad (4)$$

where θ is the scattering angle between e^- and τ^- . The four form-factors are given as

$$\begin{aligned} F_0(s) &= 1 + 2g_{V_e}g_{V_\tau}\text{Re}\chi(s) + (g_{V_e}^2 + g_{A_e}^2)(g_{V_\tau}^2 + g_{A_\tau}^2)|\chi(s)|^2, \\ F_1(s) &= 2g_{A_e}g_{A_\tau}\text{Re}\chi(s) + 4g_{V_e}g_{A_e}g_{V_\tau}g_{A_\tau}|\chi(s)|^2, \\ F_2(s) &= 2g_{V_e}g_{A_\tau}\text{Re}\chi(s) + 2(g_{V_e}^2 + g_{A_e}^2)g_{V_\tau}g_{A_\tau}|\chi(s)|^2, \\ F_3(s) &= 2g_{A_e}g_{V_\tau}\text{Re}\chi(s) + 2g_{V_e}g_{A_e}(g_{V_\tau}^2 + g_{A_\tau}^2)|\chi(s)|^2. \end{aligned} \quad (5)$$

Here, g_{V_l} and g_{A_l} are the vector and axial-vector coupling constants, respectively, of leptons l to Z^0 . The function $\chi(s)$ can be written using the mass of Z^0 (M_Z), its width (Γ_Z) and the

weak mixing angle (θ_W) as

$$\chi(s) = \frac{1}{4 \sin^2 \theta_W \cos^2 \theta_W} \times \frac{s}{s - M_Z^2 + is\Gamma_Z/M_Z}. \quad (6)$$

Integrating Eq. (4) over the full solid angle, the polarization and its forward-backward asymmetry can be expressed as

$$\begin{aligned} \mathcal{P}_\tau &= -\frac{F_2}{F_0}, \\ A_{\mathcal{P}} &= -\frac{3 F_3}{4 F_0}. \end{aligned} \quad (7)$$

Since the term including $|\chi(s)|$ are small at the TRISTAN energy, \mathcal{P}_τ is sensitive to $g_{Ve}g_{A\tau}$, and $A_{\mathcal{P}}$ to $g_{Ae}g_{V\tau}$. On the other hand, they are sensitive to A_τ and A_e , respectively at the Z^0 pole, where A_l is defined as $\mathcal{A}_l \equiv 2g_{Vl}g_{Al}/(g_{Vl}^2 + g_{Al}^2)$. In this sense, the present measurement is complementary to those from the experiments at the pole.

2 The VENUS Detector

Since the VENUS detector is described in detail elsewhere [5], we briefly summarize those components relevant to the present measurement. The central drift chamber (CDC) is the main component for charged particle tracks, located in a uniform magnetic field of 0.75 T parallel to the beam axis produced by a superconducting solenoid. Charged particles with $|\cos\theta| \leq 0.75$ (θ is the angle with respect to the beam axis) are detected in the CDC with a momentum resolution of $\sigma_p/p \approx 0.008p_t(\text{GeV}/c)$, where p_t is the transverse momentum with respect to the beam axis. The angular resolution is $8 \sin^2\theta$ mrad and 1 mrad for polar and azimuthal angles, respectively. A large cylindrical transition radiation detector (TRD) surrounds the CDC and covers an angular region of $|\cos\theta| \leq 0.68$. It provides an e/π discrimination capability as demonstrated in Fig. 1.

Between the solenoid coil and the TRD, 96 time-of-flight (TOF) counters are located at a radius of 1.66 m. A time resolution of 200 ps is obtained for charged particles within $|\cos\theta| \leq 0.78$. A cylindrical array of 5160 lead-glass blocks (LG) is located outside the solenoid in order to measure the energy of electrons and photons within $|\cos\theta| \leq 0.80$. Its good energy resolution (3.8% for 30GeV electrons) makes it possible to identify electrons and π^0 clearly. Outside the iron return yoke, eight layers of muon chambers (MU) are stacked, of which six inner layers are aligned along the beam direction, while the outermost two layers are stacked orthogonal to the inner ones. In the present analysis, the inner six layers are used for muon identification in an angular range of $|\cos\theta| \leq 0.5$.

3 Selection of τ decays

The selection of the τ decay of a specific mode proceeded in two steps. First, an preselection was made to reject non- τ events such as two-photon collision ($\gamma\gamma$ events) and multihadron events. The τ pair events are characterized with such topology as low-multiplicity, back-to-back narrow jets. The criteria of the preselection are as follows:

- 1) The number of CDC tracks should be between two and eight, where only those tracks with p_t greater than 0.2 GeV/ c coming from the interaction region are counted inside $|\cos\theta| \leq 0.50$.
- 2) The total visible energy, the sum of the track momenta and the calorimeter energies must be greater than $0.2\sqrt{s}$.
- 3) The total energy deposited in the calorimeters must be smaller than $0.8\sqrt{s}$.
- 4) The invariant mass calculated inside each of two hemispheres with respect to the thrust axis must be smaller than 4.0 GeV/ c^2 .
- 5) The acollinearity angle between the jet axes, defined by the vector sum of track momenta and energy flows in each hemisphere must be smaller than 40° .

The conditions were effective to reject $\gamma\gamma$ events (2 and 5), Bhabha events (3) and multihadronic events (4).

In the second step, decay modes into a single-prong final state were identified independently in each hemisphere. The decay modes considered here are $\tau \rightarrow e\nu\bar{\nu}$, $\mu\nu\bar{\nu}$, $\pi(K)\nu$ and $\rho\nu$, the sum of which amounts to 75 % of all τ decays.

$\tau \rightarrow \mu\nu\bar{\nu}$: The muons were identified by using the MU. The tracks which were associated with at least four corresponding hit layers of the MU were identified as μ . Those events in which both hemispheres were identified as $\mu\nu\bar{\nu}$ were discarded to reject $ee \rightarrow \mu\mu$ and $ee\mu\mu$ events.

$\tau \rightarrow \rho\nu$: For the non- μ tracks, the energy deposit in the TRD (E_{TRD}) was required to be smaller than 10 keV to ensure the track to be π^\pm . Those tracks which were associated with one or two neutral energy clusters in the LG inside a 30° cone were taken as candidates of ρ . Figure 2a) shows the invariant mass distribution of the selected two clusters. A peak corresponding to π^0 is clearly seen above small background. We selected those pairs whose invariant mass lies within 35 MeV/ c^2 around the π^0 mass as candidates. Any single isolated cluster was taken as π^0 whose decay gammas merged into one cluster. Finally, the invariant mass of the π^\pm and the π^0 candidates were calculated. Its distribution is shown in Fig. 2b). We selected those which lie within 230 MeV/ c^2 around the ρ mass as

$\rho\nu$ decay candidates.

$\tau \rightarrow e\nu\bar{\nu}$: The electrons were identified by using the LG and TRD information [6]. Among the tracks not selected in the preceding identifications, the candidate tracks were selected by requiring E/p , the ratio of energy deposit in the LG to the track momentum, to be greater than 0.8. E_{TRD} was also required to exceed 10 keV to assure the passage of electron. Those events in which both hemispheres were identified as a $e\nu\bar{\nu}$ decay were removed in order to reject Bhabha events and $ee \rightarrow eeee$ events.

$\tau \rightarrow \pi(K)\nu$: Among those tracks which were associated with no substantial MU hits (one hit layer was allowed), π^\pm tracks were selected by requiring $E/p < 0.8$ and $E_{\text{TRD}} < 10$ keV. They were also required to have no neutral clusters with energy greater than 200 MeV within 60° around them. Since π/K separation was not possible in the present analysis, $\tau \rightarrow K\nu$ mode was also included in this category.

Application of the TRD, which is one of the unique features of the VENUS detector, assures reliable identification among $e\nu\bar{\nu}$, $\rho\nu\bar{\nu}$ and $\pi\nu$ decay modes.

The number of the selected decays and the estimated background are summarized in Table 1. The efficiencies and contaminations for the above identification procedures were evaluated as a function of the daughter particle momentum, using real data from other processes: $ee \rightarrow ee$, $ee\gamma$ and $eeee$ as the electron sample; $ee \rightarrow \mu\mu$, $\mu\mu\gamma$, $ee\mu\mu$ and cosmic rays as the muon sample; $ee \rightarrow ee\pi\pi$, $\tau \rightarrow 3\pi\nu$ and $K_s \rightarrow 2\pi$ as the pion sample. It was found that there were no apparent momentum dependence in the efficiencies nor contaminations. They are also summarized in Table 1. For a confirmation, the branching ratios evaluated from our data are also listed together with the world average [7]. Those are in good agreements with one another.

4 Evaluation of the polarization and its asymmetry

In the case of the three body decays of τ leptons such as $\tau \rightarrow e\nu\bar{\nu}$ or $\mu\nu\bar{\nu}$, the energy spectrum of the charged leptons is expressed as [8]

$$\frac{df}{dx} = a(x) + \mathcal{P}_\tau b(x), \quad (8)$$

where $a(x) = (5 - 9x^2 + 4x^3)/3$, $b(x) = (1 - 9x^2 + 8x^3)/3$ and x is the laboratory energy of the charged lepton scaled to the beam energy. Figure 3 shows the observed x distributions for a) $e\nu\bar{\nu}$ and b) $\mu\nu\bar{\nu}$ modes.

For the two body decays such as $\tau \rightarrow \pi\nu$ or $\rho\nu$, the momentum spectrum of the decay particle is expressed in the same way as [8]

$$\frac{df}{dx} = 1 + \alpha\mathcal{P}_\tau(2x - 1) \quad (9)$$

where α is an analyzing power related to the spin of the final state ($\alpha=1$ for $\pi\nu$ mode and $\alpha=0.46$ for $\rho\nu$ mode). Figure 3c) shows the observed spectra for $\pi\nu$ mode. The smaller analyzing power for the $\rho\nu$ mode, which comes from the mixture of opposite polarization states of ρ , can be restored by introducing a second kinematical variable [9] to discriminate the polarization state. In the present analysis, we used the decay angle of ρ in the τ rest frame relative to the τ flight direction ($\cos\psi_\tau \approx 2x - 1$) and the decay angle of the charged π in the ρ rest frame relative to the ρ flight direction ($\cos\psi_\rho$). The $\cos\psi_\rho$ distribution was examined in two $\cos\psi_\tau$ regions, $\cos\psi_\tau < 0$ and $\cos\psi_\tau > 0$, separately. The observed distributions are shown in Fig. 4.

The polarization was evaluated by fitting the linear combination of the kinematical distributions expected for the full polarization cases ($h = \pm 1$) to the corresponding observed distributions. The fit was done by minimizing a χ^2 defined as

$$\chi^2 = \sum_i \left[\frac{N_i^{\text{meas}} - \frac{1}{2}[(1 + \mathcal{P}_\tau)(N_i^+ + N_i^{\text{BG}+}) + (1 - \mathcal{P}_\tau)(N_i^- + N_i^{\text{BG}-})]}{\sigma_i} \right]^2, \quad (10)$$

where N_i^{meas} is the number of entries in i -th bin, N_i^+ (N_i^-) and $N_i^{\text{BG}+}$ ($N_i^{\text{BG}-}$) are those of Monte Carlo events with $h = +1$ (-1) for the signal and the background coming from other decay modes of τ , respectively. The denominator, σ_i is the statistical error in each bin. The expected contributions from non- τ process were subtracted from N_i^{meas} beforehand.

The Monte Carlo events for each helicity state of τ leptons were generated by using KORALZ 4.0 [10] for τ pair production and TAUOLA2.5 [11] for τ decay. The radiative effect in the initial state, which affects the energy spectra substantially, is properly incorporated up to $O(\alpha^2)$ in the event generation. The efficiencies in the decay mode identifications were treated according to the functions evaluated in the previous section. The results of the fit are shown in Figs. 3 and 4 with histograms. The average polarizations of τ thus evaluated are tabulated in Table 2.

The forward-backward asymmetry of the polarization, $A_{\mathcal{P}}$, was evaluated by the same procedure as above in the forward ($0 \leq \cos\theta < 0.5$) and backward ($-0.5 < \cos\theta < 0$) region, separately. The scattering angle was determined by the thrust axis of the event and the charge of the daughter particle. From the forward and backward polarization thus evaluated, its asymmetry was calculated as listed in Table 3.

The systematic errors in the above measurements were considered in three categories.

Detection efficiency: The evaluation of polarization can be affected by uncertainties in the momentum dependence of the efficiency of the decay mode identification. Since the estimation was made using real data, there are substantial statistical uncertainties. Their effects on \mathcal{P}_τ were estimated by changing the efficiency independently in each momentum bin within their errors.

Background: Uncertainties related to the background, either from mis-identified τ decays or non- τ processes, can lead to the systematic error. The evaluation were found to be very stable with the possible variation of the background fraction.

Monte Carlo statistics: Because of limited statistics in the Monte Carlo simulation, the generated spectra had some uncertainties. The systematic errors due to them were estimated by changing the number of entries in each bin of the spectra within their statistical errors.

The systematic errors thus estimated are summarized in Table 2 and Table 3. As found in the tables, the systematic errors are significantly smaller than the statistical ones in the present analysis.

Combining the results for all the modes studied in the present analysis with neglecting the small systematic errors safely, the average polarization of τ leptons and its forward-backward asymmetry are

$$\mathcal{P}_\tau = 0.012 \pm 0.058, \quad (11)$$

$$A_{\mathcal{P}} = 0.029 \pm 0.057. \quad (12)$$

Although the present results are consistent with zero and are also consistent with the values predicted by the Standard Model (0.028 and 0.021, respectively, at $\sqrt{s} = 58$ GeV), they are the first substantial measurements in the energy region below the Z^0 pole as found in Fig. 5, where the results from the present and the previous experiments are plotted together with the standard model prediction.

5 Conclusions

The polarization of τ leptons and its forward-backward asymmetry in the reaction $e^+e^- \rightarrow \tau^+\tau^-$ have been measured at the center-of-mass energy of 58 GeV. They are evaluated to be 0.012 ± 0.058 and 0.029 ± 0.057 , respectively, combining the results for all the decay modes studied. The prediction of the standard model is confirmed in the energy region below the Z^0 pole.

Acknowledgment

We wish to thank the TRISTAN machine group for their patient efforts regarding the accelerator operation that continued for many years. We gratefully acknowledge the outstanding contributions of the technical staff at KEK and the collaborating institutes who participated in the construction and operation of the VENUS detector. The data acquisition and analyses were made possible with continuous support by people from the on-line group and the computer center of KEK. We thank K. Hagiwara for useful discussions. Thanks also go to Z. Was for his help to use the KORALZ and the TAUOLA Monte Carlo generators.

References

- [1] H. D. Dahmen, L. Schülke and G. Zech, Phys. Lett. **81B**(1979)361; Z. Phys. **C5**(1980)71;
G. Goggi, Proc. of LEP Summer Study, CERN 79-01 (1979)483;
S. Jadach and Z. Was, Z Physics at LEP 1, Volume 1, CERN 89-08(1989)235.
- [2] ALEPH Collaboration, D. Buskulic *et al.*, Z. Phys. **C69**(1996)183;
DELPHI Collaboration, P. Abreu *et al.*, Z. Phys. **C67**(1995)183;
OPAL Collaboration, R. Akers *et al.*, Z. Phys. **C65**(1995)1;
L3 Collaboration, M. Acciarri *et al.*, Phys. Lett. **341**(1994)245.
- [3] MAC Collaboration, W. T. Ford *et al.*, Phys. Rev. **D36**(1987)1971;
CELLO Collaboration, H. J. Behrend *et al.*, Phys. Lett. **127B**(1983)270;
AMY Collaboration, M. H. Lee *et al.*, KEK Preprint 90-70(1990).
- [4] S. Weinberg, Phys. Rev. Lett. **19**(1967)1264; A. Salam, Proc. 8th Nobel Symposium, ed.
N. Svartholm, p. 367 (Stockholm, 1968).
- [5] R. Arai *et al.*, Nucl. Instr. and Meth. **A217**(1983)181; K. Ogawa *et al.*, Nucl. Instr.
and Meth. **A243**(1986)58; T. Sumiyoshi *et al.*, Nucl. Instr. and Meth. **A271**(1988)432;
Y. Hemmi *et al.*, Jpn. J. Appl. Phys. **26**(1987)982; H. Saito *et al.*, Nucl. Instr. Meth.
A281(1989)462; K. Amako *et al.*, Nucl. Instr. and Meth. **A272**(1988)687; M. Sakuda *et al.*,
Nucl. Instr. and Meth. **A311**(1992)57; N. Terunuma *et al.*, Nucl. Instr. and Meth.
A323(1992)471; T. Arima *et al.*, Phys. Rev. **D55**(1997)19.
- [6] A. Krüger *et al.*, Nucl. Instr. and Meth. **A340**(1994)501.
- [7] Particle Data Group, Phys. Rev. **D54**(1996).
- [8] Y. S. Tsai, Phys. Rev. **D4**(1971)2821.
- [9] K. Hagiwara, A. D. Martin and D. Zeppenfeld, Phys. Lett. **B235**(1990)198;
A. Rougé, Z. Phys. **C8**(1990)75.
- [10] KORALZ4.0, S. Jadach, B. F. L. Ward, Z. Was, Comp. Phys. Commun. **79**(1994)503.
- [11] TAUOLA2.5, S. Jadach, Z. Was, R. Decker, J. H. Kuhn, Comp. Phys. Commun.
76(1993)361.

Table 1: The number of identified decays, the estimated background contribution and the selection efficiency for each decay mode. Also listed are calculated branching ratios and corresponding PDG96 values.

	$\rho\nu$	$\pi(K)\nu$	$e\nu\bar{\nu}$	$\mu\nu\bar{\nu}$
# observed	829	287	564	628
# background(τ)	75.6 ± 8.1	25.9 ± 1.6	2.0 ± 0.4	6.2 ± 0.8
# background(non- τ)	17.7 ± 2.4	8.7 ± 1.6	20.3 ± 4.0	21.7 ± 1.9
Efficiency(%)	36.1 ± 1.0	24.3 ± 0.8	34.5 ± 1.0	41.3 ± 1.3
BR(%)	$24.1 \pm 0.9 \pm 0.8$	$12.3 \pm 0.8 \pm 0.5$	$18.6 \pm 0.8 \pm 0.7$	$17.2 \pm 0.7 \pm 0.6$
PDG96(%)	25.24 ± 0.16	12.03 ± 0.14	17.83 ± 0.08	17.35 ± 0.10

Table 2: Evaluated \mathcal{P}_τ and systematic errors contributing to it. Errors indicated in the first column represent statistical ones.

	$e\bar{\nu}\nu$	$\mu\bar{\nu}\nu$	$\pi(K)\nu$	$\rho\nu$
\mathcal{P}_τ	0.13 ± 0.18	0.15 ± 0.20	-0.01 ± 0.12	-0.03 ± 0.07
Efficiency	0.021	0.021	0.018	0.024
τ BG	0.014	0.013	0.010	0.009
Non- τ BG	0.012	0.008	0.009	0.011
Monte Carlo statistics.	0.021	0.020	0.013	0.015
Total systematic error	0.035	0.033	0.026	0.032

Table 3: Evaluated $A_{\mathcal{P}}$ and systematic errors contributing to it. Errors indicated in the first column represent statistical ones.

	$e\bar{\nu}\nu$	$\mu\bar{\nu}\nu$	$\pi(K)\nu$	$\rho\nu$
$A_{\mathcal{P}}$	-0.02 ± 0.17	-0.01 ± 0.19	0.03 ± 0.12	0.04 ± 0.07
Efficiency	0.023	0.025	0.017	0.026
τ BG	0.015	0.012	0.011	0.009
Non- τ BG	0.013	0.008	0.010	0.014
Monte Carlo statistics.	0.022	0.019	0.015	0.013
Total systematic error	0.038	0.035	0.027	0.033

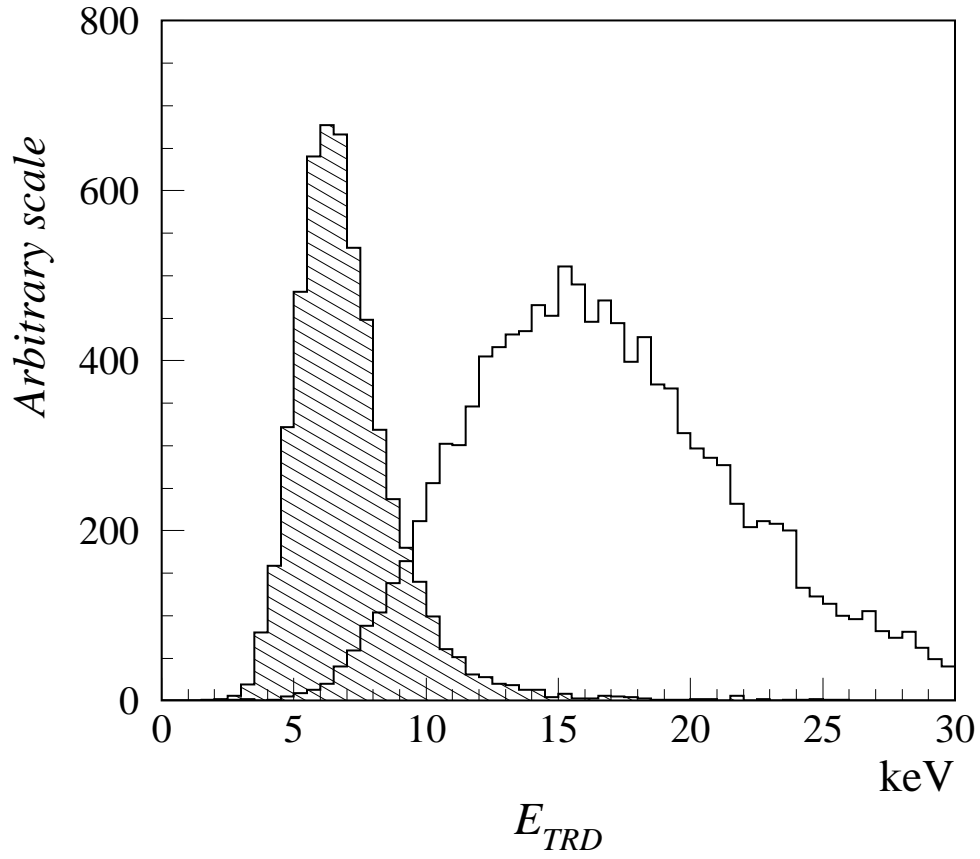


Figure 1: Energy deposit spectra in the TRD, for electrons (solid line histogram) and for muons (hatched histogram) with their momenta greater than 2 GeV/ c . The spectrum for pions must be the same as that for muons. The cut at 10 keV provides a clear discrimination between electrons and pions.

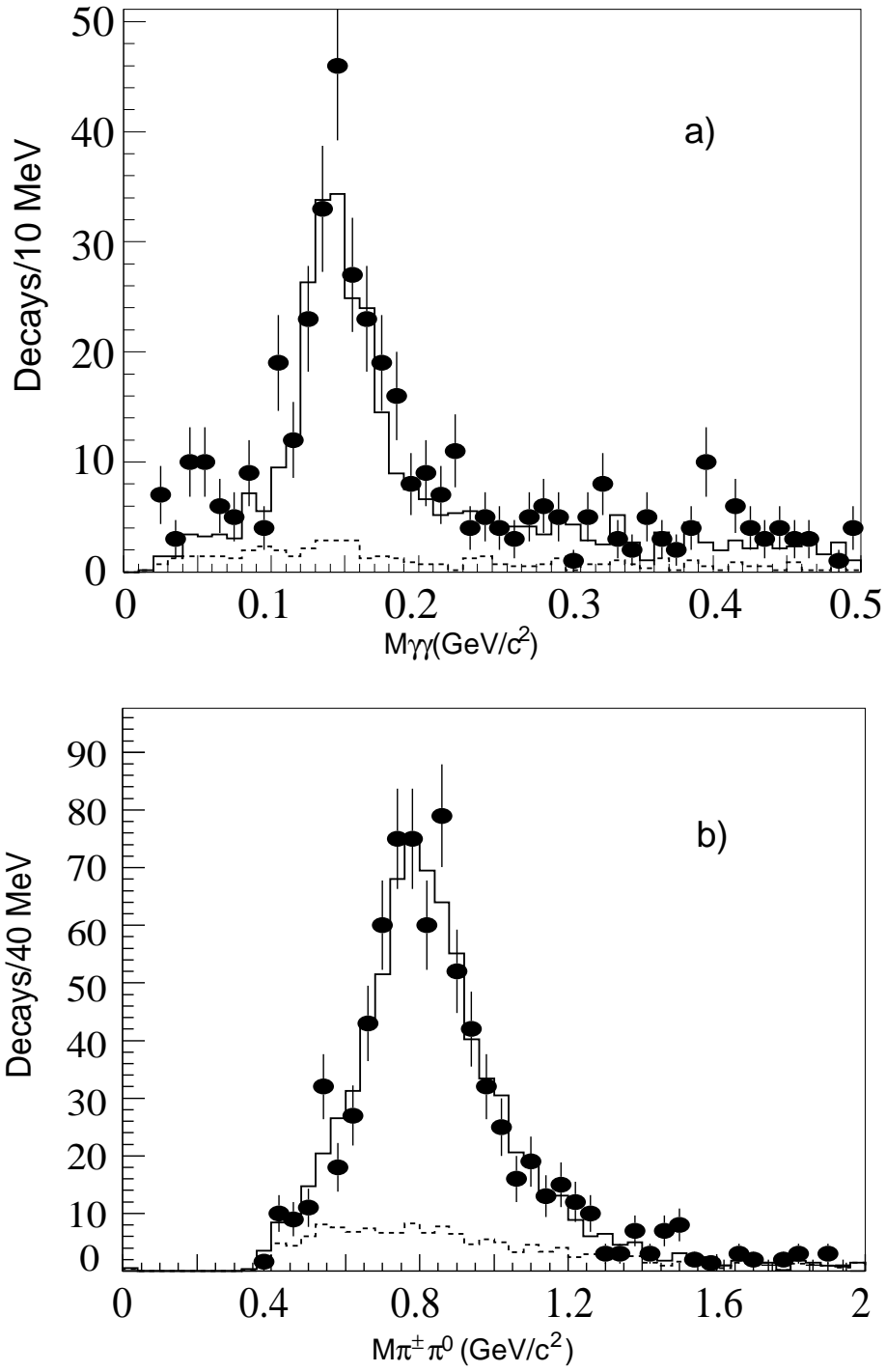


Figure 2: Invariant mass distribution of a) the two photons and b) $\pi^{\pm}\pi^0$ in the selection of the $\rho\nu$ decay mode. The solid histogram shows the simulation result. The estimated background contributions are indicated with the dashed histogram.

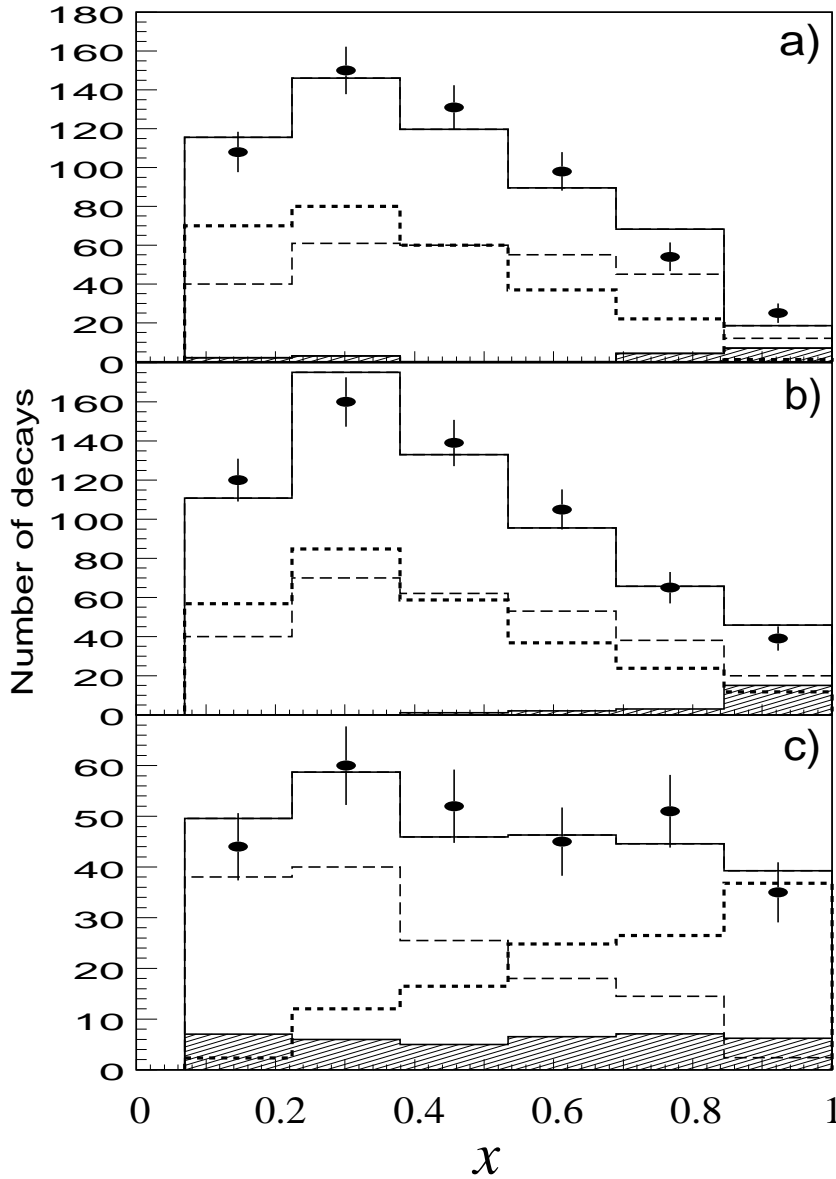


Figure 3: Scaled energy distribution for a) $\tau \rightarrow e\nu\bar{\nu}$, b) $\mu\nu\bar{\nu}$ and c) $\pi\nu\bar{\nu}$ modes. The filled circles indicate the selected candidates. The solid line histograms represent the result of the fit. Contributions from each helicity state are indicated by the dashed ($h = +1$) and dotted ($h = -1$) histograms. The background contributions are illustrated with the shaded histogram.

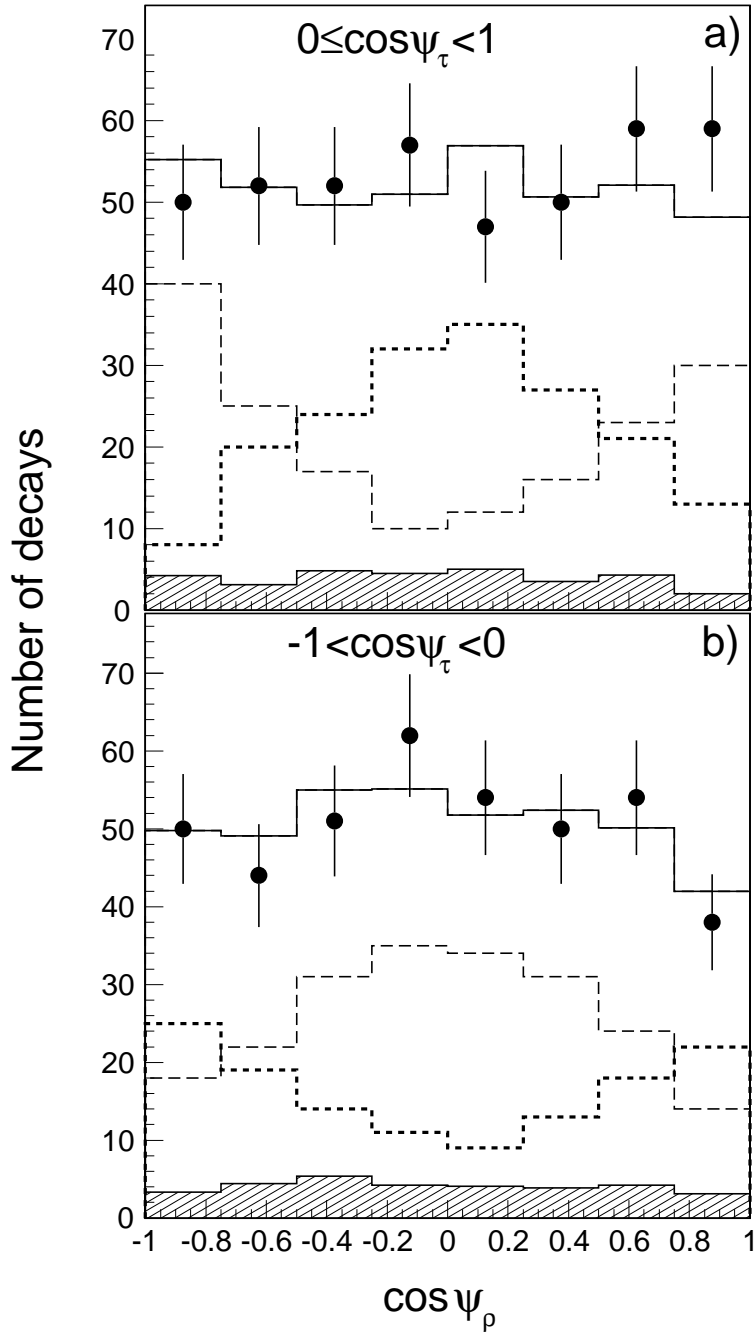


Figure 4: Observed $\cos \psi_\rho$ distributions for the $\tau \rightarrow \rho \nu$ candidates in the region of a) $0 < \cos \psi_\tau$ and b) $\cos \psi_\tau < 0$. The filled circles indicate the selected candidate. The solid line histograms represent the result of the fit. Contributions from each helicity state are indicated by the dashed ($h = +1$) and dotted ($h = -1$) histograms. The background contributions are illustrated with the shaded histogram.

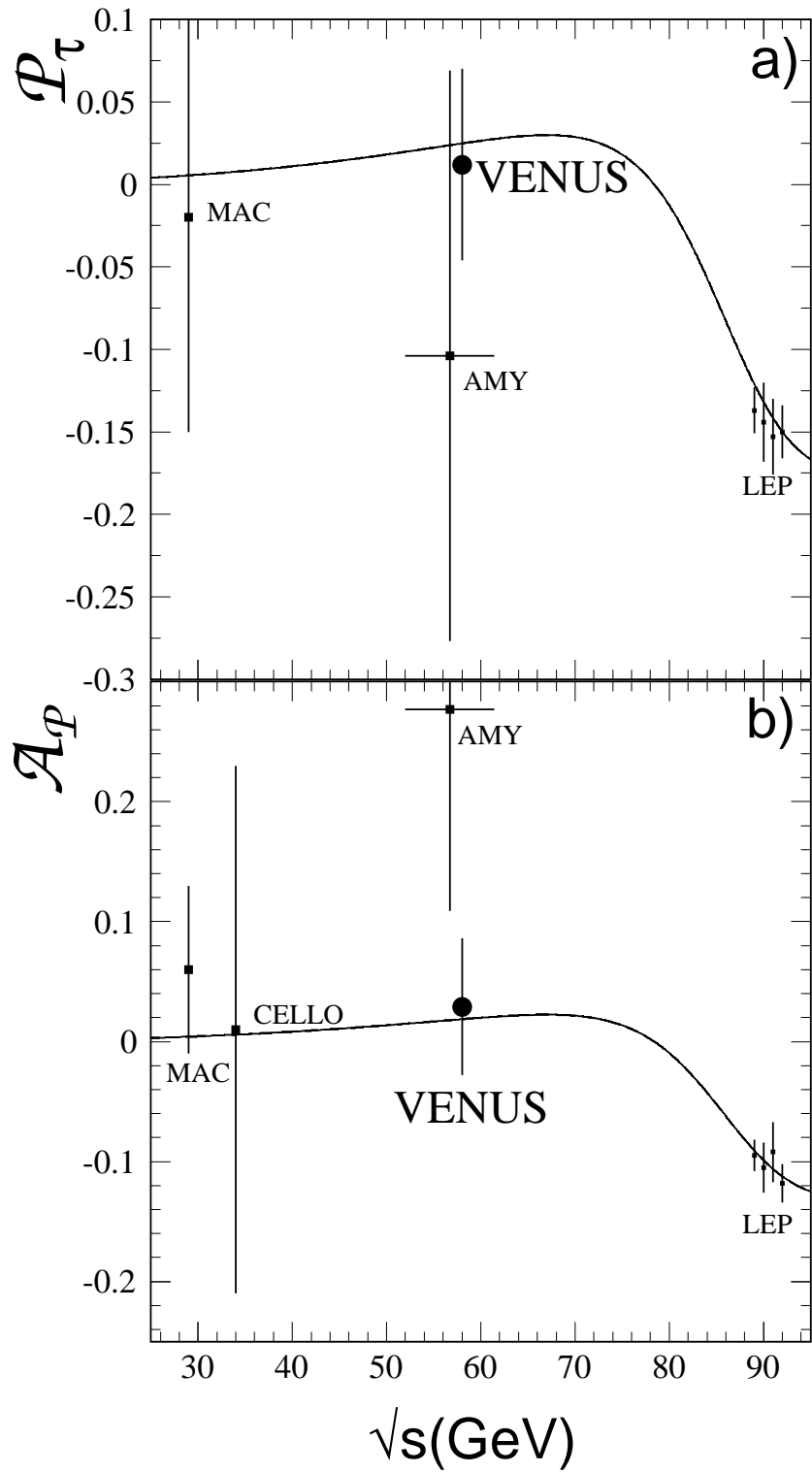


Figure 5: Measured a) average polarization \mathcal{P}_τ and b) polarization asymmetry \mathcal{A}_P together with those from other experiments. Solid line indicates the Standard Model prediction.